




## Article

# Efficient Charge Transfer Channels in Reduced Graphene Oxide/Mesoporous TiO<sub>2</sub> Nanotube Heterojunction Assemblies toward Optimized Photocatalytic Hydrogen Evolution

Zhenzi Li <sup>†</sup>, Decai Yang <sup>†</sup>, Hongqi Chu, Liping Guo, Tao Chen, Yifan Mu, Xiangyi He, Xueyan Zhong, Baoxia Huang, Shiyu Zhang, Yue Gao, Yuxiu Wei, Shijie Wang <sup>\*</sup> and Wei Zhou <sup>\* </sup>

Shandong Provincial Key Laboratory of Molecular Engineering, School of Chemistry and Chemical Engineering, Qilu University of Technology (Shandong Academy of Sciences), Jinan 250353, China; zzli@q lu.edu.cn (Z.L.); decaiyang@q lu.edu.cn (D.Y.); hongqichu@q lu.edu.cn (H.C.); lipingguo@q lu.edu.cn (L.G.); taochen@q lu.edu.cn (T.C.); yifanmou@q lu.edu.cn (Y.M.); xiangyihe@q lu.edu.cn (X.H.); xueyanzhong@q lu.edu.cn (X.Z.); baoxiahuang@q lu.edu.cn (B.H.); shiyuzhang@q lu.edu.cn (S.Z.); yuegao123@q lu.edu.cn (Y.G.); yuxiuwei@q lu.edu.cn (Y.W.)

<sup>\*</sup> Correspondence: wsj0924@q lu.edu.cn (S.W.); wzhou@q lu.edu.cn (W.Z.)

<sup>†</sup> These authors contributed equally to this work.

**Abstract:** Interface engineering is usually considered to be an efficient strategy to promote the separation and migration of photoexcited electron-hole pairs and improve photocatalytic performance. Herein, reduced graphene oxide/mesoporous titanium dioxide nanotube heterojunction assemblies (rGO/TiO<sub>2</sub>) are fabricated via a facile hydrothermal method. The rGO is anchored on the surface of TiO<sub>2</sub> nanosheet assembled nanotubes in a tightly manner due to the laminated effect, in which the formed heterojunction interface becomes efficient charge transfer channels to boost the photocatalytic performance. The resultant rGO/TiO<sub>2</sub> heterojunction assemblies extend the photoresponse to the visible light region and exhibit an excellent photocatalytic hydrogen production rate of 932.9 μmol<sup>-1</sup> g<sup>-1</sup> under simulated sunlight (AM 1.5G), which is much higher than that of pristine TiO<sub>2</sub> nanotubes (768.4 μmol h<sup>-1</sup> g<sup>-1</sup>). The enhancement can be ascribed to the formation of a heterojunction assembly, establishing effective charge transfer channels and favoring spatial charge separation, the introduced rGO acting as an electron acceptor and the two-dimensional mesoporous nanosheets structure supplying a large surface area and adequate surface active sites. This heterojunction assembly will have potential applications in energy fields.

**Keywords:** TiO<sub>2</sub>; photocatalysis; mesoporous structure; assembly; heterojunction



**Citation:** Li, Z.; Yang, D.; Chu, H.; Guo, L.; Chen, T.; Mu, Y.; He, X.; Zhong, X.; Huang, B.; Zhang, S.; et al. Efficient Charge Transfer Channels in Reduced Graphene Oxide/Mesoporous TiO<sub>2</sub> Nanotube Heterojunction Assemblies toward Optimized Photocatalytic Hydrogen Evolution. *Nanomaterials* **2022**, *12*, 1474. <https://doi.org/10.3390/nano12091474>

Academic Editor: Nikos Tagmatarchis

Received: 26 March 2022

Accepted: 23 April 2022

Published: 26 April 2022

**Publisher's Note:** MDPI stays neutral with regard to jurisdictional claims in published maps and institutional affiliations.



**Copyright:** © 2022 by the authors. Licensee MDPI, Basel, Switzerland. This article is an open access article distributed under the terms and conditions of the Creative Commons Attribution (CC BY) license (<https://creativecommons.org/licenses/by/4.0/>).

## 1. Introduction

In recent years, the energy crisis and environmental pollution have become two major topics in the field of science and technology research [1,2]. The development and utilization of new technology has become the primary task of current research. Among various options, photocatalysis is favored for its low carbon footprint and use of renewable resources [3–5]. The most important thing is that it can directly use solar energy to generate new energy, such as hydrogen energy, and plays an important role in the degradation of pollutants and nitrogen fixation [6]. Therefore, it is considered to be an efficient strategy to solve the current increasingly serious environmental problems, and it has good application prospects.

In 1972, Honda and Fujishima [7] discovered that titanium dioxide (TiO<sub>2</sub>) could cause photocatalytic water-splitting. Since then, many scholars have begun to conduct a large number of experimental studies on TiO<sub>2</sub> [8]. So far, TiO<sub>2</sub> has obviously become the most widely studied photocatalyst due to its advantages of high stability and activity, super hydrophilicity, low cost and environmental friendliness in the field of photocatalysis [9,10]. However, from the perspective of the mechanism, it can be found that TiO<sub>2</sub> has three

fatal defects, which seriously limit its development. Firstly, TiO<sub>2</sub> has a large band gap energy (3.2 eV), which means that the photogenerated electron-hole can only be activated by ultraviolet light with an energy higher than 3.2 eV (wavelength less than 387 nm), which only accounts for ~5% of sunlight. It was clear that visible light with a relatively long wavelength (almost 43% of sunlight) could not stimulate the photocatalytic activity of TiO<sub>2</sub> [11,12]. Secondly, the excited photogenerated electrons and holes in TiO<sub>2</sub> have a strong oxidability and reducibility, which leads to a rapid recombination and inefficient quantum efficiency. Studies have shown that most (about 90%) of the excited photogenerated electrons and holes of TiO<sub>2</sub> have recombined before photocatalysis [13]. Thirdly, traditional TiO<sub>2</sub> materials have a low specific surface area, which restricts the photocatalytic activity of TiO<sub>2</sub> obviously [14,15].

In recent years, some methods have been adopted to improve the photocatalytic performance of TiO<sub>2</sub>. Firstly, the surface area of TiO<sub>2</sub> could be improved by adjusting the morphology [16]. In addition, an excellent morphology can also improve the probability of charge transport by shortening the transmission path [17]. Secondly, TiO<sub>2</sub> is modified by doping, metal deposition, and recombination to improve its activity. Doping can be used for improving the charge transfer efficiency and can be used for dragging down the bandgap [18]. Metal deposition can either form a Schottky barrier or an Ohmic contact, improving the efficiency of charge separation [19], and the introduction of metal can also broaden the absorption of light into the visible light region [20]. Recombination can improve charge separation efficiency through electron transfer [21]. Among various methods, heterojunction construction is a simple and practical method to effectively promote charge separation [22–24]. Graphene, as a representative of two-dimensional carbon materials, is composed of a single layer of carbon atoms with an sp<sup>2</sup> hybrid orbital in the shape of a hexagonal honeycomb [25]. Graphene oxide (GO) is prepared by embedding O atoms into the c-scaffold of graphene to make sp<sup>2</sup> and sp<sup>3</sup> domains exist simultaneously in the structure, which promotes the expansion of multiple interactions. On this basis, reduced graphene oxide (rGO) can provide more interfacial polarization sites and absorption sites [26]. Thus, rGO has obvious application prospects in many fields including energy and environment, along with thermal and electrical properties [27–29]. In recent years, some reports had been reported on the application of rGO/TiO<sub>2</sub> composite materials in the field of photocatalysis. Balsamo et al. successfully prepared a TiO<sub>2</sub>-rGO composite structure using the one-pot method by solar irradiation, which is simple and green. The degradation rate of 2,4-dichlorophenoxyacetic acid after irradiation for 3 h reached 97%. The enhanced absorption of the composite is due to the interaction between the TiO<sub>2</sub> and rGO [30]. Zouzelka et al. optimized rGO/TiO<sub>2</sub> composites by electrophoretic deposition. The presence of rGO can, to some extent, promote the photocatalytic degradation of 4-chlorophenol. Compared with TiO<sub>2</sub>, the photocatalytic degradation rate of the composite material is several times higher, and this enhanced performance is due to the charge transfer promoting the formation of hydroxyl radical [31]. Firstly, rGO could change the band gap width of TiO<sub>2</sub> to expand its light response range. Secondly, it can be used as an electron transporter, which can effectively prevent photogenerated electron hole recombination and significantly prolong the lifetime of the electron-hole pair. In addition, a large specific surface area can provide more active sites for photocatalytic reactions [32]. Therefore, rGO/TiO<sub>2</sub> composite materials maybe have good application prospects in the field of photocatalysis due to their high charge separation efficiency. Although these rGO/TiO<sub>2</sub> composites indeed improved the photocatalytic performance obviously, they are still far from being practical applications. The question of how to further promote the charge separation of rGO/TiO<sub>2</sub>-based materials via interface engineering is still a great challenge.

Here, novel reduced graphene oxide/mesoporous titanium dioxide nanotube heterojunction assemblies (rGO/TiO<sub>2</sub>) are fabricated via a facile hydrothermal method by utilizing mesoporous TiO<sub>2</sub> nanosheet-assembled nanotubes as the host. For one thing, the morphology of TiO<sub>2</sub> was regulated into the nanotube structure assembled by the mesoporous nanosheet, which increased the specific surface area of the material and exposed

more active sites. Besides, a tubular structure increased the multiple reflection of sunlight inside the tube and improved the utilization rate of light. For another thing, rGO, as an electron acceptor, was introduced to form rGO/TiO<sub>2</sub> heterojunction assemblies, which contributed to improve the spatial charge separation efficiency and extend the photore-sponse to the visible light region. The rGO/TiO<sub>2</sub> heterojunction assemblies significantly improved the photocatalytic activity, and the photocatalytic hydrogen production rate was up to 932.9  $\mu\text{mol h}^{-1} \text{g}^{-1}$ , 1.2 times higher than that of pristine TiO<sub>2</sub>. The novel rGO/TiO<sub>2</sub> heterojunction assemblies may provide new insights for the fabrication of TiO<sub>2</sub>-based photocatalysts with a high performance.

## 2. Materials and Methods

### 2.1. Chemicals

Titanium oxysulfate (TiOSO<sub>4</sub>), potassium permanganate (KMnO<sub>4</sub>), sodium nitrate (NaNO<sub>3</sub>) and sulfuric acid (H<sub>2</sub>SO<sub>4</sub>) were purchased from Aladdin Chemical (Shanghai, China). Ethanol (EtOH), ether (C<sub>2</sub>H<sub>5</sub>OC<sub>2</sub>H<sub>5</sub>) and glycerol (C<sub>3</sub>H<sub>5</sub>(OH)<sub>3</sub>) were purchased from Tianjin Kermio Chemical (Tianjin, China). None of the chemicals were further purified.

### 2.2. Preparation of TiO<sub>2</sub> Nanotube

The typical method for the synthesis of a TiO<sub>2</sub> nanotube is based on the literature, and the specific steps are as follows [33]. 1 g TiOSO<sub>4</sub> was added to 18 mL EtOH with intense stirring for 30 min, after which 9 mL C<sub>3</sub>H<sub>5</sub>(OH)<sub>3</sub> and 9 mL C<sub>2</sub>H<sub>5</sub>OC<sub>2</sub>H<sub>5</sub> were added drop by drop, stirred overnight, and then transferred to the Teflon reactor at 170 °C for 10 h. After the reaction, the obtained precursor was collected by repetitive centrifugation at 8000 rpm for 10 min and washed several times by deionized water and ethanol and dried at 60 °C for 12 h. After drying, the samples were transferred to a Muffle furnace and kept at 600 °C for 4 h. Finally, the TiO<sub>2</sub> nanotube sample was obtained.

### 2.3. Preparation of rGO/TiO<sub>2</sub>

The formation process of rGO/TiO<sub>2</sub> is shown in Figure 1a. rGO/TiO<sub>2</sub> samples are synthesized on the basis of TiO<sub>2</sub>, and rGO is prepared by the hummer method using KMnO<sub>4</sub>, NaNO<sub>3</sub> and H<sub>2</sub>SO<sub>4</sub> as raw materials [34,35]. The prepared 5 mg rGO was added to 18 mL EtOH, stirred and ultrasonicated for 20 min, after which 1 g TiOSO<sub>4</sub> was added. Then, 9 mL C<sub>3</sub>H<sub>5</sub>(OH)<sub>3</sub> and 9 mL C<sub>2</sub>H<sub>5</sub>OC<sub>2</sub>H<sub>5</sub> were added drop by drop, stirred overnight, and transferred to the Teflon-lined autoclave at 170 °C for 10 h. After the reaction, the resulting product was centrifuged and washed with deionized water and anhydrous ethanol 3 times and dried for later use. After drying, the samples were transferred to a Muffle furnace for calcination at 600 °C for 4 h. Finally, rGO/TiO<sub>2</sub> samples were obtained. According to the feeding ratio, the content of rGO on TiO<sub>2</sub> is 1 wt%.

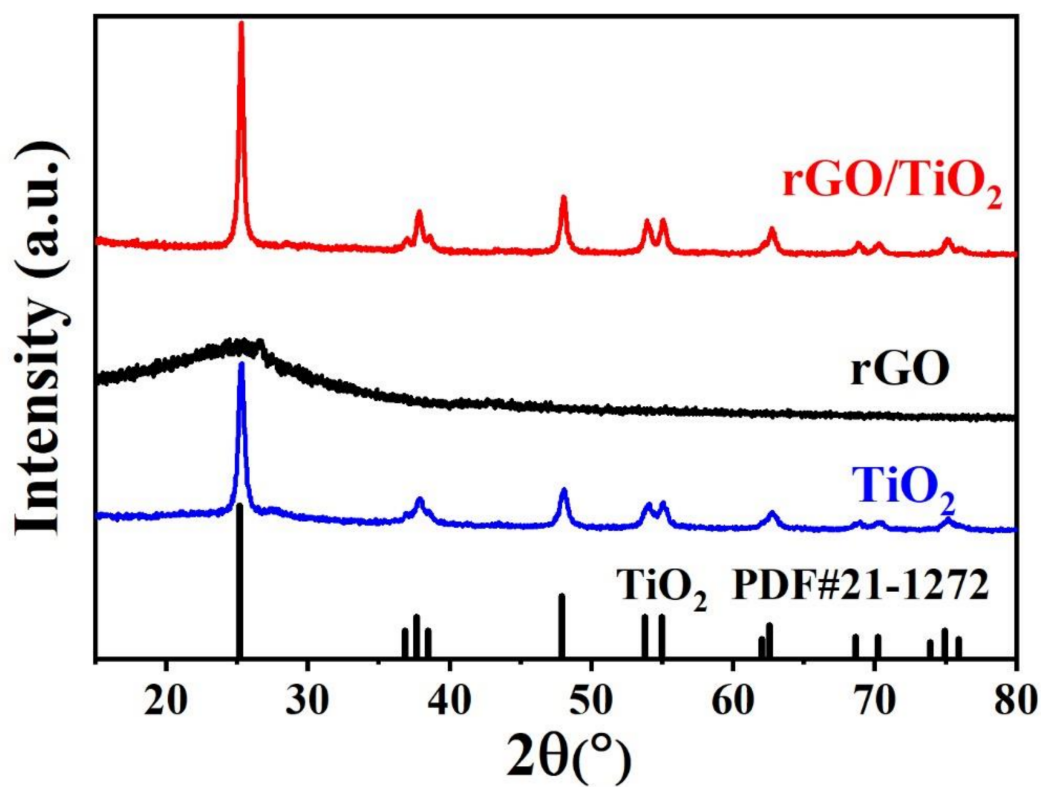
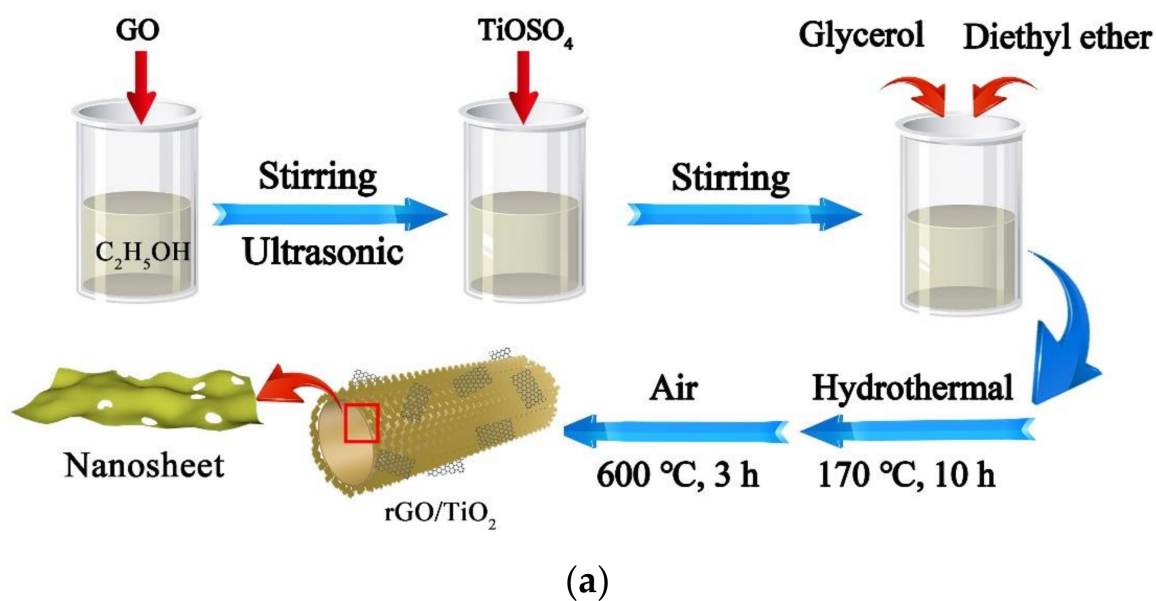
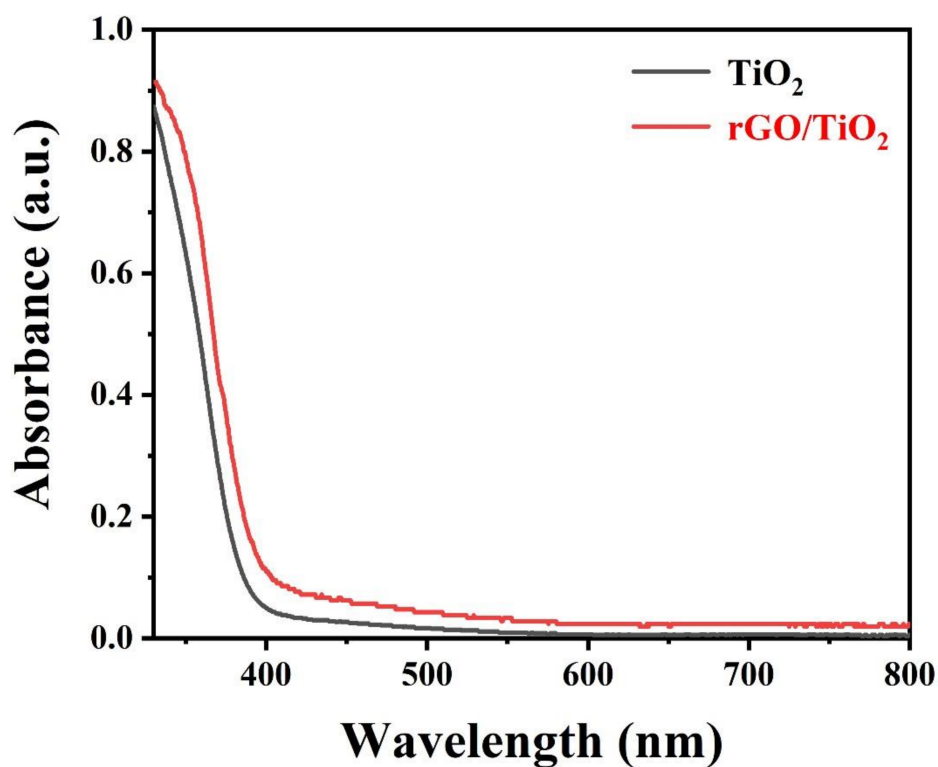
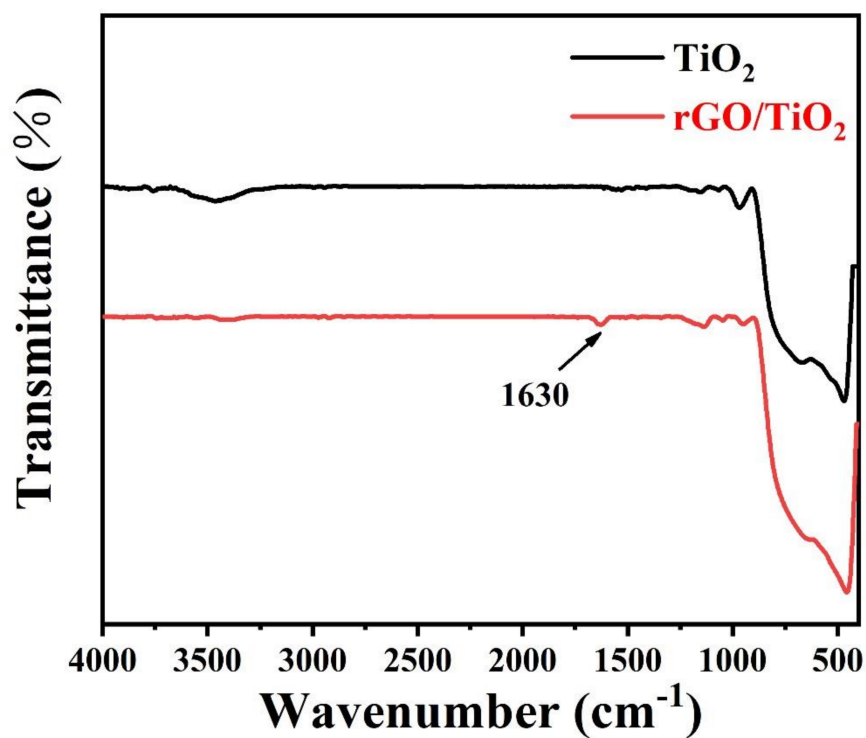


Figure 1. Cont.



(c)



(d)

**Figure 1.** Schematic representation of the formation of (a)  $\text{rGO/TiO}_2$  heterojunction assembly photocatalysts; (b) X-ray diffraction (XRD) patterns, (c) UV-visible diffuse reflectance spectra, and (d) FTIR of  $\text{TiO}_2$  and  $\text{rGO/TiO}_2$ , respectively.

### 3. Results and Discussion

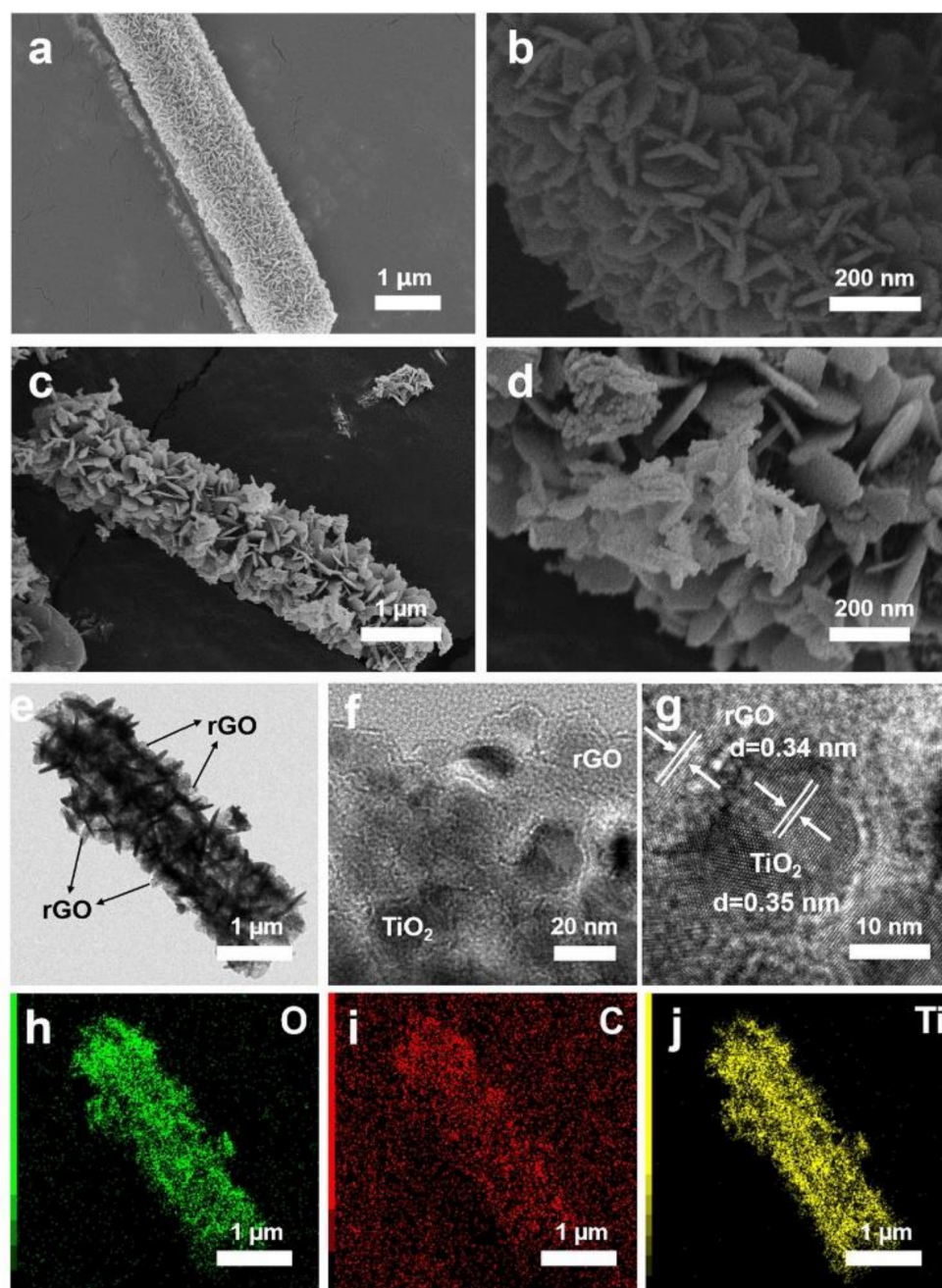
#### 3.1. Crystal Structure and Optical Absorption of rGO/TiO<sub>2</sub>

Figure 1b shows the X-ray diffraction (XRD) patterns of GO, TiO<sub>2</sub> and GO/TiO<sub>2</sub>. The multiple diffraction peaks located at 25.3, 37.8, 48.0, 55.1, 62.8, 70.2 and 75.0° can be assigned to the (101), (004), (200), (211), (204), (116) and (220) planes of anatase TiO<sub>2</sub> (JCPDS 21-1272), respectively [36]. This indicates the successful preparation of anatase TiO<sub>2</sub>. The characteristic peak positions of rGO (Figure 1b and Figure S1) are about 26° and 42.5°, which is consistent with the literature [37]. Figure 1b shows the XRD pattern of the rGO/TiO<sub>2</sub> composite material, which is basically consistent with that of TiO<sub>2</sub>, indicating that the introduction of rGO does not destroy the crystal structure of TiO<sub>2</sub>. This also implies the stability of the material. However, the increased strength of the (101) crystal plane preliminarily indicates the successful introduction of rGO. The reason for this stems from the coincidence of the position of the TiO<sub>2</sub> (101) crystal plane (25.3°) and rGO (26°), and no single peak of rGO can be observed. As shown in Figure 1c, UV-vis was applied to obtain the absorption property of the materials. TiO<sub>2</sub> has a strong light absorption capacity when the wavelength is less than 400 nm, which is the inherent absorption property of crystal anatase TiO<sub>2</sub>. The absorption intensity of rGO/TiO<sub>2</sub> was higher than that of TiO<sub>2</sub>, indicating the enhancement of the composites. The photoresponse region of the material extended the UV absorption to the visible light region, which was attributed to the modification of rGO. Figure 1d shows FTIR of TiO<sub>2</sub> and rGO/TiO<sub>2</sub>, the principal vibration of TiO<sub>2</sub> corresponding to the wide band in the range of 400–800 cm<sup>-1</sup>. The significant band at 670 cm<sup>-1</sup> corresponds to the bending vibration mode of the Ti–O–Ti bond. For the rGO/TiO<sub>2</sub> heterostructure, the wide absorption at low frequencies is similar to the spectrum of the TiO<sub>2</sub> and can therefore be attributed to the vibration of the TiO<sub>2</sub>. In addition, the peak broadening of rGO/TiO<sub>2</sub> relative to TiO<sub>2</sub> below 1000 cm<sup>-1</sup> may be due to the superposition of the peak existing in the Ti–O–C vibration (798 cm<sup>-1</sup>) on Ti–O–Ti. The emerging absorption band at around 1630 cm<sup>-1</sup> can be associated with the bone vibration of the graphene sheet, indicating the successful loading of rGO [38]. The weak peak was due to the low amount of rGO on the TiO<sub>2</sub> surface (about 1 wt%).

#### 3.2. Morphology of rGO/TiO<sub>2</sub> Assembly

A scanning electron microscope (SEM, Hitachi, S-4800, Tokyo, Japan) and transmission electron microscope (TEM, JEOL, JEM-2100, Tokyo, Japan) were used to observe the microstructure of TiO<sub>2</sub> and rGO/TiO<sub>2</sub>. It can be clearly seen that TiO<sub>2</sub> shows a very uniform tubular structure, assembled by many sheets, with a diameter of about 700 nm (Figure 2a,b). Compared with TiO<sub>2</sub>, the surface of rGO/TiO<sub>2</sub> becomes slightly rough, and the diameter of the tube increases slightly (Figure 2c,d). The sheet structure can increase the specific surface area and expose more active sites. The tubular structure formed by the self-assembly of multiple nanosheets can further increase the specific surface area of the material. Secondly, the tubular structure can reflect and utilize the sunlight efficiently, which improves the utilization rate of light and is conducive to improving the photocatalytic activity. In addition, the heterostructure formed by TiO<sub>2</sub> and rGO is beneficial to the electron transfer between materials, which reduces the electron-hole recombination rate and improves the charge separation efficiency and photocatalytic activity. TEM images of rGO/TiO<sub>2</sub>, as shown in Figure 2e, illustrate a nanosheet-assembled tubular structure, and the light-colored part on the surface is a layer of rGO, which is consistent with the results obtained by SEM. The rGO could be anchored on the surface of the nanosheets due to the laminated effect, thus forming efficient heterojunctions. The HRTEM images (Figure 2f,g) of rGO/TiO<sub>2</sub> show that the edge of the sample is a layer of rGO and that the inner layer is TiO<sub>2</sub>. As shown in Figure 2g, clear lattice fringes can be seen with a lattice spacing of about 0.35 nm corresponding to the (101) crystal plane of anatase TiO<sub>2</sub>. Meanwhile, it can be clearly seen that the lattice spacing of rGO is 0.34 nm, which further indicates the successful preparation of the rGO/TiO<sub>2</sub> heterojunction assembly material. Elemental mapping (Figure 2h–j) shows that O, C and

Ti elements in rGO/TiO<sub>2</sub> are evenly dispersed. The above information demonstrates the successful manufacturing of the rGO/TiO<sub>2</sub> heterojunction assembly.

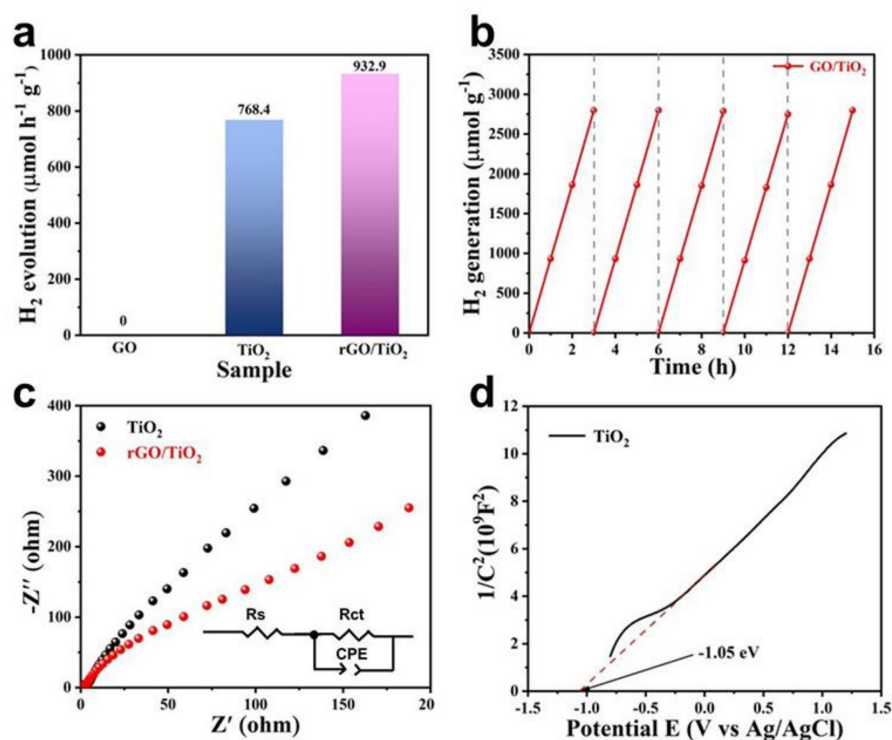


**Figure 2.** The SEM images of (a,b) TiO<sub>2</sub> and (c,d) rGO/TiO<sub>2</sub>, and the (e) TEM, (f,g) HRTEM images and (h–j) elemental mappings of the rGO/TiO<sub>2</sub> heterojunction assembly.

### 3.3. Photocatalytic Performance of rGO/TiO<sub>2</sub>

The photocatalytic performance of the catalysts for hydrogen production under favorable conditions of the catalyst Pt was conducted. As shown in Figure 3a, the hydrogen production performance of rGO is nearly 0, indicating that the presence of rGO does not contribute to hydrogen production, which is consistent with the reports in the literature. The hydrogen production quantity of rGO/TiO<sub>2</sub> is 932.9 μmol h<sup>-1</sup> g<sup>-1</sup>, which is 1.2 times higher than that of original TiO<sub>2</sub> (768.4 μmol h<sup>-1</sup> g<sup>-1</sup>). We can clearly see the excellent photocatalytic performance of rGO/TiO<sub>2</sub>, which is significantly better than in the previous literature (Table S1). This is mainly attributed to the formation of a heterojunction between

TiO<sub>2</sub> and rGO, which promotes the spatial charge separation and inhibits the recombination of electron-hole pairs. Secondly, the design of an rGO sheet supported on a TiO<sub>2</sub> sheet is more conducive to external proton reduction. This 2D/2D design can also maximize the interface contact area, integrate the advantages of each 2D component, and facilitate the photocatalytic reaction. Finally, the nanosheet-assembled tubular structure provides a large specific surface area and sufficient surface active sites for the photocatalytic reaction. Under sunlight irradiation (AM 1.5G), the special microstructure can realize multiple reflections within the tubular structure, improving the utilization rate of sunlight. To investigate the stability of catalysts, cyclic tests were performed (Figure 3b). Five cycles of rGO/TiO<sub>2</sub> were tested, and the hydrogen production rates were almost identical for each cycle. Besides, the amount of hydrogen production was not attenuated, indicating that rGO/TiO<sub>2</sub> possessed a high stability, which was favorable for practical applications.



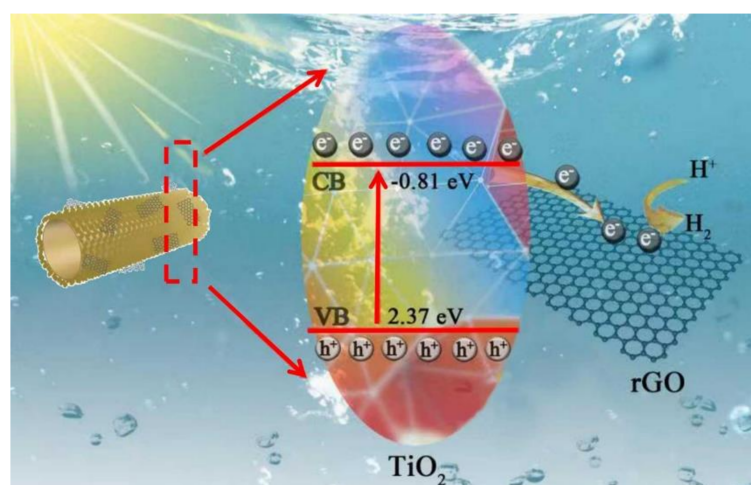
**Figure 3.** (a) Photocatalytic H<sub>2</sub> evolution rate of rGO, TiO<sub>2</sub> and rGO/TiO<sub>2</sub>, (b) recycling tests of rGO/TiO<sub>2</sub>, (c) the Nyquist plots of electrochemical impedance under AM 1.5G of TiO<sub>2</sub> and rGO/TiO<sub>2</sub>, and (d) the Mott–Schottky plots of TiO<sub>2</sub>.

Figure 3c shows the electrochemical impedance spectra (EIS, Shanghai Chenhua Instrument Co., Ltd., CHI760E, Shanghai, China) of TiO<sub>2</sub> and rGO/TiO<sub>2</sub> under AM 1.5G light irradiation. It can be clearly seen that the arc radius of the EIS diagram of rGO/TiO<sub>2</sub> is smaller than that of TiO<sub>2</sub>, indicating that rGO/TiO<sub>2</sub> has a lower electrochemical impedance under light irradiation. This result clearly indicates that there is a positive synergistic effect between TiO<sub>2</sub> and rGO on the enhancing electron migration, which has a more efficient charge carrier separation and faster electron transfer to reduce the electron-hole recombination rate and promote the photocatalytic hydrogen generation [39]. In order to analyze the semiconductor type and band structure of TiO<sub>2</sub>, the Mott–Schottky curve was tested for TiO<sub>2</sub>. As shown in Figure 3d, the slope of the curve is positive, which is typical for n-type semiconductors [40]. At the same time, the flat band potential of TiO<sub>2</sub> (−1.05 eV) can be obtained from the slope of the curve, and the conduction band of TiO<sub>2</sub> is −0.81 eV [41]. Combined with UV-vis, the valence band position is determined at 2.31 eV.



### 3.4. Photocatalytic Mechanism of rGO/TiO<sub>2</sub>

Based on the above, the mechanism diagram of photocatalytic hydrogen production of the rGO/TiO<sub>2</sub> heterojunction was made, as shown in Scheme 1. When the rGO/TiO<sub>2</sub> catalyst is irradiated by light, the electrons on TiO<sub>2</sub> are excited to the conduction band (CB), leaving holes in the valence band (VB). Meanwhile, TiO<sub>2</sub> will come into contact with rGO to form a built-in electric field. Since rGO is an electron acceptor, electrons will transfer from TiO<sub>2</sub> CB to rGO. Additionally, the reduction reaction H<sup>+</sup> converts to H<sub>2</sub> on rGO. The improved photocatalytic performance is attributed to an electron derived from the rGO/TiO<sub>2</sub> heterojunction, which reduces the recombination and improves the spatial charge separation efficiency. Such high photocatalytic properties are inseparable from the structure itself. The nanosheet-assembled hollow tubular structures provide a large specific surface area and adequate surface active sites for photocatalytic reactions. In addition, the nanotube structure can improve the utilization rate of light energy. The reason for this is that light can be reflected and used multiple times in the cavity. These factors all contribute to improving the photocatalytic hydrogen evolution of the rGO/TiO<sub>2</sub> heterojunction assembly.



**Scheme 1.** The mechanism diagram of photocatalytic hydrogen production of the rGO/TiO<sub>2</sub> heterojunction assembly.

## 4. Conclusions

In summary, an rGO/TiO<sub>2</sub> heterojunction assembly was prepared by a step hydrothermal method, and the H<sub>2</sub> production rate was much faster than that of the original TiO<sub>2</sub> nanotubes under AM 1.5G irradiation. This was mainly decided by the following two aspects. Firstly, the rGO heterostructure with TiO<sub>2</sub> promoted the electron transfer, reduced the electron recombination rate, and improved the spatial charge efficiency. The design of rGO sheets supported by TiO<sub>2</sub> sheets is more conducive to the reduction of external protons. Secondly, the advantage of the special structure was that the nanosheet-assembled hollow tube provided a large specific surface area. The combination of the two 2D structures maximizes the interface contact area and exposes enough reaction sites on the surface, which is favorable for photocatalytic hydrogen production. This novel strategy provides new ideas for the fabrication of other heterojunction photocatalysts with an efficient solar energy conversion.

**Supplementary Materials:** The following supporting information can be downloaded at: <https://www.mdpi.com/article/10.3390/nano12091474/s1>. Characterizations, Photocatalytic activity, Photoelectrochemical measurements [42–47]. Figure S1: XRD patterns of rGO, Table S1: Comparison with other TiO<sub>2</sub> and rGO composite catalysts.

**Author Contributions:** Conceptualization, Z.L., S.W. and W.Z.; methodology, D.Y.; software, L.G.; validation, T.C., Y.M. and X.H.; formal analysis, X.Z.; investigation, H.C.; resources, B.H.; data curation, S.Z., Y.W. and Y.G.; writing—original draft preparation, Z.L. and D.Y.; writing—review and editing, S.W. and W.Z.; visualization, W.Z.; supervision, S.W. and W.Z.; project administration, W.Z.; funding acquisition, W.Z. All authors have read and agreed to the published version of the manuscript.

**Funding:** This work was financially supported by the National Natural Science Foundation of China (Grant Number: 21871078, 52172206); the Shandong Province Natural Science Foundation (Grant Number: ZR2021MB016), and the Development plan of Youth Innovation Team in Colleges and Universities of Shandong Province.

**Data Availability Statement:** Data presented in this article are available at request from the corresponding author.

**Conflicts of Interest:** The authors declare no conflict of interest.

## References

1. Uddin, N.; Zhang, H.; Du, Y.; Jia, G.; Wang, S.; Yin, Z. Structural-phase catalytic redox reactions in energy and environmental applications. *Adv. Mater.* **2020**, *32*, 1905739. [[CrossRef](#)] [[PubMed](#)]
2. Jeong, G.; Sasikala, S.; Yun, T.; Lee, G.; Lee, W.; Kim, S. Nanoscale assembly of 2d materials for energy and environmental applications. *Adv. Mater.* **2020**, *32*, 1907006. [[CrossRef](#)] [[PubMed](#)]
3. Fang, B.; Xing, Z.; Sun, D.; Li, Z.; Zhou, W. Hollow semiconductor photocatalysts for solar energy conversion. *Adv. Powder Mater.* **2022**, *1*, 100021. [[CrossRef](#)]
4. Wang, W.; Deng, C.; Xie, S.; Li, Y.; Zhang, W.; Sheng, H.; Chen, C.; Zhao, J. Photocatalytic c–c coupling from carbon dioxide reduction on copper oxide with mixed-valence copper(I)/copper(II). *J. Am. Chem. Soc.* **2021**, *143*, 2984–2993. [[CrossRef](#)] [[PubMed](#)]
5. Jian, S.; Tian, Z.; Hu, J.; Zhang, K.; Zhang, L.; Duan, G.; Yang, W.; Jiang, S. Enhanced visible light photocatalytic efficiency of La-doped ZnO nanofibers via electrospinning-calcination technology. *Adv. Powder Mater.* **2022**, *1*, 100004. [[CrossRef](#)]
6. Ma, B.; Blanco, M.; Calvillo, L.; Chen, L.; Chen, G.; Lau, T.-C.; Dražić, G.; Bonin, J.; Robert, M.; Granozzi, G. Hybridization of Molecular and Graphene Materials for CO<sub>2</sub> Photocatalytic Reduction with Selectivity Control. *J. Am. Chem. Soc.* **2021**, *143*, 8414–8425. [[CrossRef](#)]
7. Fujishima, A.; Honda, K. Electrochemical Photolysis of Water at a Semiconductor Electrode. *Nature* **1972**, *238*, 37–38. [[CrossRef](#)]
8. Gong, H.; Wang, L.; Zhou, K.; Zhang, D.; Zhang, Y.; Adamaki, V.; Bowen, C.; Sergejevs, A. Improved photocatalytic performance of gradient reduced TiO<sub>2</sub> ceramics with aligned pore channels. *Adv. Powder Mater.* **2021**, *1*, 100025. [[CrossRef](#)]
9. Qiu, P.; Li, W.; Thokchom, B.; Park, B.; Cui, M.; Zhao, D.; Khim, J. Uniform core–shell structured magnetic mesoporous TiO<sub>2</sub> nanospheres as a highly efficient and stable sonocatalyst for the degradation of bisphenol-A. *J. Mater. Chem. A* **2015**, *3*, 6492–6500. [[CrossRef](#)]
10. Hao, Z.; Chen, Q.; Dai, W.; Ren, Y.; Zhou, Y.; Yang, J.; Xie, S.; Shen, Y.; Wu, J.; Chen, W.; et al. Oxygen-deficient blue TiO<sub>2</sub> for ultrastable and fast lithium storage. *Adv. Energy Mater.* **2020**, *10*, 1903107. [[CrossRef](#)]
11. Wang, H.; Hu, X.; Ma, Y.; Zhu, D.; Li, T.; Wang, J. Nitrate-Group-Grafting-Induced Assembly of Rutile TiO<sub>2</sub> Nanobundles for Enhanced Photocatalytic Hydrogen Evolution. *Chin. J. Catal.* **2020**, *41*, 95–102. [[CrossRef](#)]
12. Yu, L.; Zhang, G.; Liu, C.; Lan, H.; Liu, H.; Qu, J. Interface Stabilization of Undercoordinated Iron Centers on Manganese Oxides for Nature-Inspired Peroxide Activation. *ACS Catal.* **2018**, *8*, 1090–1096. [[CrossRef](#)]
13. Skinner, D.; Colombo, D.; Cavaleri, J.; Bowman, R. Femtosecond Investigation of Electron Trapping in Semiconductor Nanoclusters. *J. Phys. Chem.* **1995**, *99*, 7853–7856. [[CrossRef](#)]
14. Lan, K.; Liu, Y.; Zhang, W.; Liu, Y.; Elzatahry, A.; Wang, R.; Xia, Y.; Al-Dhayan, D.; Zheng, N.; Zhao, D. Uniform Ordered Two-Dimensional Mesoporous TiO<sub>2</sub> Nanosheets from Hydrothermal-Induced Solvent-Confined Monomicelle Assembly. *J. Am. Chem. Soc.* **2018**, *140*, 4135–4143. [[CrossRef](#)]
15. Zhao, Y.; Zhao, Y.; Shi, R.; Wang, B.; Waterhouse, G.I.N.; Wu, L.; Tung, C.; Zhang, T. Tuning Oxygen Vacancies in Ultrathin TiO<sub>2</sub> Nanosheets to Boost Photocatalytic Nitrogen Fixation up to 700 nm. *Adv. Mater.* **2019**, *31*, 1806482. [[CrossRef](#)]
16. Wu, J.; Qiao, P.; Li, H.; Xu, Y.; Yang, W.; Yang, F.; Lin, K.; Pan, K.; Zhou, W. Engineering surface defects on two-dimensional ultrathin mesoporous anatase TiO<sub>2</sub> nanosheets for efficient charge separation and exceptional solar-driven photocatalytic hydrogen evolution. *J. Mater. Chem. C* **2020**, *8*, 3476. [[CrossRef](#)]
17. Bae, D.; Pedersen, T.; Seger, B.; Malizia, M.; Kuznetsov, A.; Hansen, O.; Chorkendorff, I.; Vesborg, P. Back-illuminated Si photocathode: A combined experimental and theoretical study for photocatalytic hydrogen evolution. *Energy Environ. Sci.* **2015**, *8*, 650–660. [[CrossRef](#)]
18. Yi, L.; Ci, S.; Luo, S.; Shao, P.; Hou, Y.; Wen, Z. Scalable and Low-cost Synthesis of Black Amorphous Al-Ti-O Nanostructure for High-efficient Photothermal Desalination. *Nano Energy* **2017**, *41*, 600–608. [[CrossRef](#)]
19. Bae, D.; Kanellos, G.; Faasse, G.M.; Dražević, E.; Venugopal, A.; Smith, W.A. Design principles for efficient photoelectrodes in solar rechargeable redox flow cell applications. *Commun. Mater.* **2020**, *1*, 17. [[CrossRef](#)]

20. Abed, J.; Rajput, N.S.; El Moutaouakil, A.; Jouiad, M. Recent Advances in the Design of Plasmonic Au/TiO<sub>2</sub> Nanostructures for Enhanced Photocatalytic Water Splitting. *Nanomaterials* **2020**, *10*, 2260. [[CrossRef](#)]
21. Song, W.; Ji, J.; Guo, K.; Wang, X.; Wei, X.; Cai, Y.; Tan, W.; Li, L.; Sun, J.; Tang, C.; et al. Solid-phase impregnation promotes Ce doping in TiO<sub>2</sub> for boosted denitration of CeO<sub>2</sub>/TiO<sub>2</sub> catalysts. *Chin. Chem. Lett.* **2022**, *33*, 935–938. [[CrossRef](#)]
22. Zhu, Y.; Shah, M.; Wang, C. Insight into the role of Ti<sup>3+</sup> in photocatalytic performance of shuriken-shaped BiVO<sub>4</sub>/TiO<sub>2-x</sub> heterojunction. *Appl. Catal. B Environ.* **2017**, *203*, 526–532. [[CrossRef](#)]
23. Wang, H.; Liu, J.; Xiao, X.; Meng, H.; Wu, J.; Guo, C.; Zheng, M.; Wang, X.; Guo, S.; Jiang, B. Engineering of SnO<sub>2</sub>/TiO<sub>2</sub> heterojunction compact interface with efficient charge transfer pathway for photocatalytic hydrogen evolution. *Chin. Chem. Lett.* **2022**, *in press*. [[CrossRef](#)]
24. Jia, M.; Yang, Z.; Xiong, W.; Cao, J.; Xiang, Y.; Peng, H.; Jing, Y.; Zhang, C.; Xu, H.; Song, P. Magnetic heterojunction of oxygen-deficient Ti<sup>3+</sup>-TiO<sub>2</sub> and Ar-Fe<sub>2</sub>O<sub>3</sub> derived from metal-organic frameworks for efficient peroxydisulfate (PDS) photo-activation. *Appl. Catal. B Environ.* **2021**, *298*, 120513. [[CrossRef](#)]
25. Novoselov, K.S.; Geim, A.K.; Morozov, S.V.; Jiang, D.; Zhang, Y.; Dubonos, S.V.; Grigorieva, I.V.; Firsov, A.A. Electric Field Effect in Atomically Thin Carbon Films. *Science* **2004**, *306*, 666–669. [[CrossRef](#)]
26. Sharma, D.; Menon, A.; Bose, S. Graphene templated growth of copper sulphide ‘flowers’ can suppress electromagnetic interference. *Nanoscale Adv.* **2020**, *2*, 3292–3303. [[CrossRef](#)]
27. Wang, X.; Meng, G.; Zhu, C.; Huang, Z.; Qian, Y.; Sun, K.; Zhu, X. A generic synthetic approach to large-scale pristine-graphene/metal-nanoparticles hybrids. *Adv. Funct. Mater.* **2013**, *23*, 5685. [[CrossRef](#)]
28. Qiu, B.; Xing, M.; Zhang, J. Mesoporous TiO<sub>2</sub> nanocrystals grown in situ on graphene aerogels for high photocatalysis and lithium-ion batteries. *J. Am. Chem. Soc.* **2014**, *136*, 5852–5855. [[CrossRef](#)]
29. Xu, C.; Wang, C.; He, X.; Lyu, M.; Wang, S.; Wang, L. Processable graphene oxide embedded titanate nanofiber membranes with improved filtration performance. *J. Hazard. Mater.* **2017**, *325*, 214–222. [[CrossRef](#)] [[PubMed](#)]
30. Balsamo, S.; Fiorenza, R.; Condorelli, M.; Pecoraro, R.; Brundo, M.; Presti, F.; Sciré, S. One-Pot Synthesis of TiO<sub>2</sub>-rGO Photocatalysts for the Degradation of Groundwater Pollutants. *Materials* **2021**, *14*, 5938. [[CrossRef](#)]
31. Zouzelka, R.; Remzova, M.; Plšek, J.; Brabec, L.; Rathousky, J. Immobilized rGO/TiO<sub>2</sub> Photocatalyst for Decontamination of Water. *Catalysts* **2019**, *9*, 708. [[CrossRef](#)]
32. Wang, S.; Cai, J.; Mao, J.; Li, S.; Shen, J.; Gao, S.; Huang, J.; Wang, X.; Parkin, I.P.; Lai, Y. Defective black Ti<sup>3+</sup> self-doped TiO<sub>2</sub> and reduced graphene oxide composite nanoparticles for boosting visible-light driven photocatalytic and photoelectrochemical activity. *Appl. Surf. Sci.* **2019**, *467–468*, 45–55. [[CrossRef](#)]
33. Zhang, X.; Hu, W.; Zhang, K.; Wang, J.; Sun, B.; Li, H.; Qiao, P.; Wang, L.; Zhou, W. Ti<sup>3+</sup> Self-Doped Black TiO<sub>2</sub> Nanotubes with Mesoporous Nanosheet Architecture as Efficient Solar-Driven Hydrogen Evolution Photocatalysts. *ACS Sustain. Chem. Eng.* **2017**, *5*, 6894–6901. [[CrossRef](#)]
34. Marcano, D.C.; Kosynkin, D.V.; Berlin, J.M.; Sinitskii, A.; Sun, Z.; Slesarev, A.; Alemany, L.B.; Lu, W.; Tour, J.M. Improved synthesis of graphene oxide. *ACS Nano* **2010**, *4*, 4806–4814. [[CrossRef](#)]
35. Cote, L.J.; Kim, F.; Huang, J. Langmuir-blodgett assembly of graphite oxide single layers. *J. Am. Chem. Soc.* **2009**, *131*, 1043–1049. [[CrossRef](#)]
36. Yu, C.; Li, M.; Yang, D.; Pan, K.; Yang, F.; Xu, Y.; Yuan, L.; Qu, Y.; Zhou, W. NiO nanoparticles dotted TiO<sub>2</sub> nanosheets assembled nanotubes P-N heterojunctions for efficient interface charge separation and photocatalytic hydrogen evolution. *Appl. Surf. Sci.* **2021**, *568*, 150981. [[CrossRef](#)]
37. Chen, C.; Yang, S.; Ding, J.; Wang, G.; Zhong, L.; Zhao, S.; Zang, Y.; Jiang, J.; Ding, L.; Zhao, Y.; et al. Non-covalent self-assembly synthesis of AQ2S@rGO nanocomposite for the degradation of sulfadiazine under solar irradiation: The indispensable effect of chloride. *Appl. Catal. B Environ.* **2021**, *298*, 120495. [[CrossRef](#)]
38. Sang, Y.; Zhao, Z.; Tian, J.; Hao, P.; Jiang, H.; Liu, H.; Claverie, J.P. Enhanced Photocatalytic Property of Reduced Graphene Oxide/TiO<sub>2</sub> Nanobelt Surface Heterostructures Constructed by an In Situ Photochemical Reduction Method. *Small* **2014**, *18*, 3775–3782. [[CrossRef](#)]
39. Zhang, Y.; Fu, F.; Zhou, F.; Yang, X.; Zhang, D.; Chen, Y. Synergistic effect of RGO/TiO<sub>2</sub> nanosheets with exposed (001) facets for boosting visible light photocatalytic activity. *Appl. Surf. Sci.* **2020**, *510*, 145451. [[CrossRef](#)]
40. Kronik, L.; Shapira, Y. Surface photovoltage phenomena: Theory, experiment, and applications. *Surf. Sci. Rep.* **1999**, *37*, 1–206. [[CrossRef](#)]
41. Yang, F.; Li, H.; Pan, K.; Wang, S.; Sun, H.; Xie, Y.; Xu, Y.; Wu, J.; Zhou, W. Engineering Surface N-Vacancy Defects of Ultrathin Mesoporous Carbon Nitride Nanosheets as Efficient Visible-Light-Driven Photocatalysts. *Sol. RRL* **2020**, *5*, 2000610. [[CrossRef](#)]
42. Gupta, B.; Melvin, A.; Matthews, T.; Dhara, S.; Dash, S.; Tyagi, A. Facile gamma radiolytic methodology for TiO<sub>2</sub>-rGO synthesis: Effect on photo-catalytic H<sub>2</sub> evolution. *Int. J. Hydrogen Energy* **2015**, *40*, 5815–5823. [[CrossRef](#)]
43. Bharad, P.; Sivaranjani, K.; Gopinath, C. A rational approach towards enhancing solar water splitting: A case study of Au-RGO/N-RGO-TiO<sub>2</sub>. *Nanoscale* **2015**, *7*, 11206–11215. [[CrossRef](#)]
44. Ma, J.; Dai, J.; Duan, Y.; Zhang, J.; Qiang, L.; Xue, J. Fabrication of PANI-TiO<sub>2</sub>/rGO hybrid composites for enhanced photocatalysis of pollutant removal and hydrogen production. *Renew. Energy* **2020**, *156*, 1008–1018. [[CrossRef](#)]
45. Tudu, B.; Nalajala, N.; Reddy, K.; Saikia, P.; Gopinath, C. Electronic integration and thin film aspects of Au-Pd/rGO/TiO<sub>2</sub> for improved solar hydrogen generation. *ACS Appl. Mater. Inter.* **2019**, *11*, 32869–32878. [[CrossRef](#)]

46. Agegnehu, A.; Pan, C.; Tsai, M.; Rick, J.; Su, W.; Lee, J.; Hwang, B. Visible light responsive noble metal-free nanocomposite of V-doped TiO<sub>2</sub> nanorod with highly reduced graphene oxide for enhanced solar H<sub>2</sub> production. *Int. J. Hydrogen Energy* **2016**, *41*, 6752–6762. [[CrossRef](#)]
47. Wei, X.; Cao, J.; Fang, F. A novel multifunctional Ag and Sr<sup>2+</sup> co-doped TiO<sub>2</sub>@rGO ternary nanocomposite with enhanced p-nitrophenol degradation, and bactericidal and hydrogen evolution activity. *RSC Adv.* **2018**, *8*, 31822–31829. [[CrossRef](#)]